DOI: 10.13009/EUCASS2022-6129
9TH EUROPEAN CONFERENCE FOR AERONAUTICS AND SPACE SCIENCES (EUCASS)

Beyond Gravity's approach to the multidisciplinary design, analysis and optimization of reusable payload fairings

Pietro Greco, Giulio Molinari*, Marcello Righi** and Alberto Sanchez Cebrian**
**Beyond Gravity Schweiz AG*
Schaffhauserstrasse 580, 8052 Zurich, Switzerland
***ZHAW School of Engineering*
Technikumstrasse 9, 8400 Winterthur, Switzerland

Abstract
Launch vehicle payload fairings must fulfil requirements in various disciplines, from structural mechanics, thermal and acoustics to internal and external fluid-dynamics at drastically different operational conditions. Each discipline has a specific set of constraints, and the various goals are often conflicting. The proposed approach leverages multi-disciplinary analyses and optimizations, simultaneously maximizing high-level metrics such as mass and lifecycle costs by altering design parameters affecting multiple disciplines. The ability to fulfil requirements is numerically assessed from the structural, thermal, and aerodynamic perspective. Furthermore, the lifecycle cost is assessed considering the possibility of fairing reusability, and exploring different manufacturing and refurbishment strategies.

1.Introduction

The philosophy behind Space 2.0 is causing shifts in the paradigms at the basis of launch vehicle design. Megaconstellations require unprecedented number of launches, new launcher concepts – from very small to very large – are being proposed, and major private players are increasing the competitiveness in the sector. The pursue for maximum efficiency at all costs is no longer targeted. Cost-to-orbit is becoming the main metric, environmental concerns become increasingly predominant, and flexibility in launch rates and launch readiness is highly valued. All these aspects, and in particular cost reduction, are not just a simple evolution of the space market, but rather a necessity [1] to lower the barriers to access space. The drivers for launch vehicle design are therefore vastly different with respect to few decades ago, and the design of the new generation of launch vehicles is reflecting this. In this respect, the most noticeable change is the pursue of subsystems modularity and components reusability, through refurbishment or replacement. Both approaches lower the cost-to-orbit, with the latter also enabling high launch rates and reducing the environmental impact.
Achieving the ideal design of a launcher, or of one of its systems, is however a complex task, due to the great number of subsystems present, the various physical domains involved, and their mutual interaction. The design must take all needs and constraints into account, while aiming to maximize the mission goals and minimize the overall costs.
Designing and analyzing systems operating in such scenarios requires a re-think of the approaches and tools previously used. To this aim, Beyond Gravity has established a multi-disciplinary approach for the design and analysis of launcher systems, assessing their behavior from the perspective of all involved disciplines, and aiming to satisfy the complex requirements by leveraging the multidisciplinary interactions.
This paper presents the approach and its application to a conceptual low-cost reusable fairing. For this problem, it is assumed that the system shall only fulfil its aerodynamic function and not accommodate a payload. Its geometry and its subsystems, outlined in chapter 2, have been simplified as the focus of the work is to demonstrate the functionality of the proposed approach. The ultimate objective is to determine a structural architecture providing optimal performance across all disciplines while satisfying the mission requirements at minimum overall cost. In addition to coupling structural mechanics and aerothermodynamics (models described in chapter 3), the framework considers additional aspects such as the costs of materials and labor associated with manufacturing, assembling, and refurbishing the components. These interdisciplinary couplings and constraints are considered within an optimization environment (chapter 4), which accounts for their interplays in the identification of the ideal payload fairing design, satisfying the various, and often conflicting, requirements. In this study, these high-level requirements are mass and overall cost, representing key customer-centric values.

DOI: 10.13009/EUCASS2022-6129

The inputs for the study are volumetric constraints, topology and structural concepts, and trajectory profiles. The associated design parameters span all disciplines: geometry, materials choice, structural sizing and refurbishment strategy. The key requirements can be similarly formulated at a high level for each discipline (e.g. required buckling margin, maximum irradiance towards payload…) and, by nature of the coupling, this information is propagated among the affected physical domains.
Compared to performing single-disciplinary analyses, coupling structural, thermal and fluid domains increases the numerical complexity. To limit the computational effort, the multidisciplinary framework can access analysis tools characterized by different levels of fidelity and computational costs. Crucially, these models exhibit sufficient accuracy to capture the relevant phenomena, and they enable executing global, multi-disciplinary optimizations in few hours. With this holistic approach, leveraging interactions between different disciplines, a global optimum can be reached.
The outcome of the multi-objective optimization, presented in chapter 4, is a family of Pareto-optimal designs, differing in the way they attain their performance. The choice among those can be performed by relying on additional, high-level information, for example originating from the Launcher Prime business model needs, and linked to the forecasted launch cadence and pricing models.

2.Conceptual payload fairing

The conceptual payload fairing (PLF) geometry, shown in Figure 1, consists of a conical skirt and a spherical nose cap. Unlike conventional fairings, in this case there are no requirements to host a payload; consequently, the payload fairing is comprised only of the aerodynamic cone, and no cylindrical section. This geometry is referred to as “blunted-cone” and, although being rather simple, is still popular in the space industry: several commercial launchers [2] use conical shapes for their fairings.
The geometry of the rest of the launch vehicle, needed to perform Computational Fluid Dynamics (CFD) analyses, is assumed to be perfectly cylindrical, with the same radius as the payload fairing, and a length of 25 m.

2.1 Subsystems

The conceptual PLF, owing to the absence of payload, features a significantly simplified subsystem architecture with respect to conventional fairings:

- Structure:
  - Panels: the panels have a sandwich structure, with aluminum facesheets on an aluminum honeycomb core.
  - Vertical and Horizontal Separation Systems (VSS and HSS): the conceptual PLF is not required to actively separate, but needs flanges for assembly and installation. These will be only considered from a structural perspective.
- Thermal Protection System (TPS): the structure of the fairing must be protected from the aerothermal loads and – in turn – the structure shall not cause excessive irradiation towards the payload bay during the ascent. This subsystem controls the heat flow from the environment and between the various systems.
- Grounding: a low impedance path must connect all metallic parts of the fairing.
- Anti-static protection: buildup of electrostatic charges on the outer surface of the fairing must be prevented.

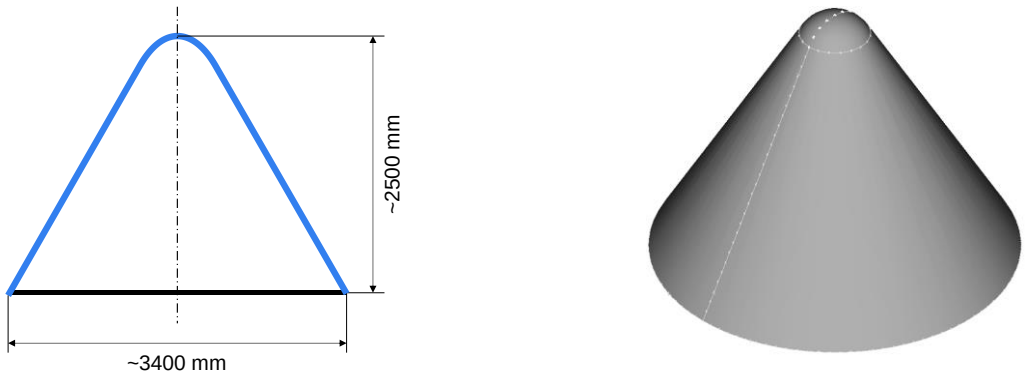

Figure 1: Overview of the fairing geometry

DOI: 10.13009/EUCASS2022-6129

2.2 Requirements

High level requirements can be defined for each subsystem, and these will be considered as hard constraints during the optimization (namely, they shall not be violated by the resulting designs). For the conceptual design presented in this contribution, only the simplified set defined in Table 1 is considered.

Table 1: Subsystems requirements

Structure – static (yield and ultimate strength)	Margin of safety on Von Mises stress ≥ 0.6
Structure – stability	Buckling factor ≥ 2
Thermal protection – maximum structural temp.	Maximum temperature for the structure ≤ 120 °C
Thermal protection – maximum irradiation	≤ 1000 W/m²
Grounding	(Satisfied through structural material choice)
Anti-static protection	(Satisfied through material treatment)

2.3 Design and materials

2.3.1 Structure

The panels that the PLF shells are made of are assumed to have a sandwich construction, with 7075 T651 aluminum alloy facesheets over a 5056 aluminum alloy honeycomb core [3]. The fairing geometry, shown in Figure 1, is single-curvature (except for the nose-cap, which is assumed to be manufactured separately in 7075 T651 aluminum alloy), and thus is well suited to this material choice and this type of construction [4]. The HSS and VSS profiles, and the nose-cap connecting ring, are also 7075 T651 aluminum alloy, and – in this preliminary phase – they are modeled as a continuous connection.
The material choice deviates from the recent trends in the space industry, which relies on CFRP facesheets and metallic cores [5, 6]. CFRP possesses favorable characteristics (drapability and ability to conform to doubly-curved surfaces, tailorable anisotropy, high strength- and stiffness-to-mass ratio); however, the costs associated to it are significantly higher than for aluminum [7].
In terms of behavior at elevated temperatures, similarly to composites, the mechanical properties of heat-treated and aged aluminum alloys decrease significantly above approximately 100 – 150 °C. The higher thermal conductivity, however, aids in reducing localized hot spots originating from aerothermal heating, and thus has the potential of reducing the requirements on the TPS[1].
The structural design is parameterized in terms of facesheet panels thickness, honeycomb core height and density. The thicknesses vary linearly in a finite number of steps (in turn, a design parameter) over the fairing height.

2.3.2 Thermal protection

The material used for the TPS is cork, adhered on the outer facesheet of the PLF panels and nose-cap. It is characterized by low thermal conductivity, low weight, and ability to absorb energy through ablation [8], characteristics that make it the industry-standard for thermal protection of launch vehicles and early reentry vehicles [9, 10].
The design of the TPS is parameterized in terms of its thickness; as with the facesheet panels, it varies linearly in a finite number of steps over the fairing height.

2.4 Conceptual mission definition

The mission considered for this work falls within the "Technology Testing" category (following the classification by Ley et al. [11]). This means that the final objective of the launch is not to deliver a payload to orbit, as for a classic mission, but rather to understand and examine new technologies and possibilities. In particular, no separation occurs during the entire launch.
The present study considers a single trajectory, derived from the launch profile of Vega. As the goal is to assess the impact on the subsystems defined in chapter 2.1, it is sufficient to consider only the longitudinal acceleration, flight path angle, and angle of attack.

[1] furthermore, the peak aerodynamic loads occur before the peak temperatures are reached. The transient thermal characteristics are therefore important in ascertaining the mechanical load-carrying capacity.

DOI: 10.13009/EUCASS2022-6129

Specifically, the assumed longitudinal acceleration profile for the launch trajectory is shown in Figure 4. It depends on several factors, in particular on the vehicle mass, fuel burn rate, engines thrust, number of stages and total drag acting on the launcher.
The fight path angle is assumed to be constant and equal to 90° up to 10 km altitude, and then to decrease linearly from 90° to 20° at 126 km altitude.
Finally, the Angle of Attack (AoA) is assumed to be zero degrees for the entire trajectory. This means that the launcher's symmetry axis is always parallel to the flow direction. This assumption is valid at supersonic Mach numbers (*Ma*). For the very first seconds of the launch, usually up to the transonic regime, the AoA might be higher than 0°. Nonetheless, given the comparatively low dynamic pressure of this phase, the assumption of zero AoA is not critical. As it will be shown in the next chapters, this assumption allows for a fundamental simplification for the CFD analyses, since it enables the use of a two-dimensional grid (for an axisymmetric analysis) rather than a three dimensional one.
With this information, the entire trajectory (shown in Figure 2 and Figure 3) can be determined, up to the final altitude of 126 km.

3.Analysis models

3.1 Structural model

The numerical model representing the PLF structure is the FE mesh shown in Figure 5. It is comprised of shell elements to model the sandwich panels (laminated shell elements) and nose cap (plate shell elements), and one-dimensional beam elements to represent the vertical and horizontal connection elements (nose cap connection profile, VSS and HSS, albeit without "separation" function, with an H-shaped cross-section).
The model is used to perform both static and linear buckling analyses, using MSC.NASTRAN as solver.
The boundary conditions for the mechanical model consist of a fully rigid fixation along the HSS, and the loads originate from the aerodynamic pressure and from the rigid body accelerations. These are obtained from the trajectory (chapter 2.4), with the addition of a 1 g lateral acceleration to account for maneuvering loads.

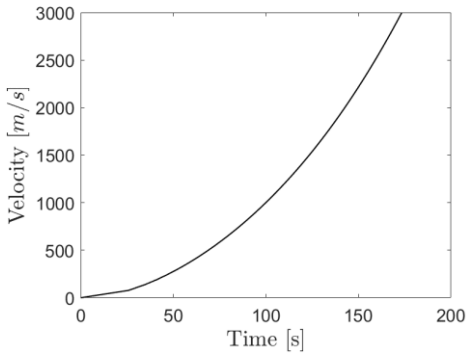

Figure 2: Launcher velocity

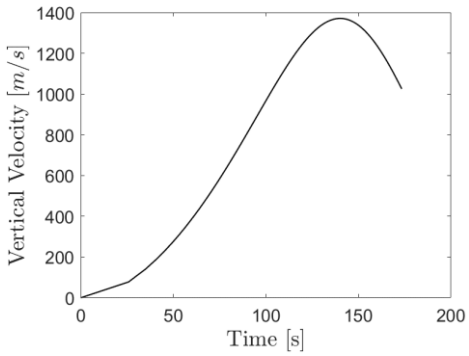

Figure 3: Launcher vertical velocity

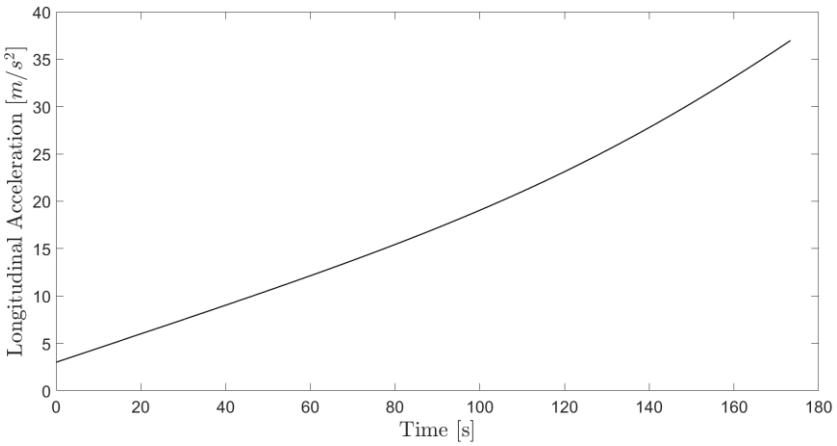

Figure 4: Launcher longitudinal acceleration

DOI: 10.13009/EUCASS2022-6129

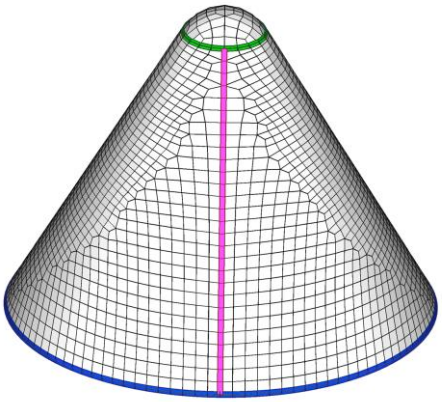

Figure 5: Structural mesh

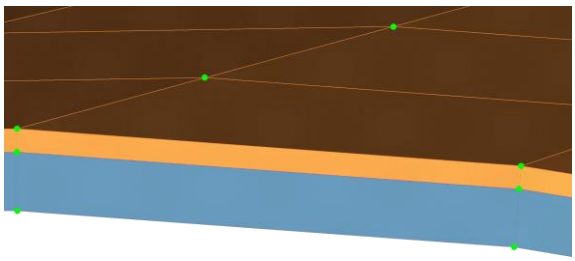

Figure 6: Thermal mesh (detail)

3.2 Thermal model

The thermal model shares the basic geometry with the structural model. Unlike it, however, it also relies on solid elements to model the sandwich panels, leading to the presence of multiple nodes along their thickness. This allows to capture the thermal gradient along the thickness. In particular, the panels have three nodes along the thickness and two linear solid elements, representing respectively the cork and the honeycomb for the skirt section, and the cork and the aluminum shell for the nose cap section. The aluminum skins are modeled with two-dimensional shell elements, contributing to the in-plane heat transfer: given the high thermal conductivity of aluminum and the limited thickness of the skins, it is safe to assume that the through-thickness temperature gradient is negligible.
The mesh of the thermal model is shown in Figure 6: the brown solid elements represent the cork layer; the light blue solid elements represent the honeycomb core, and the FE nodes are shown in green. The light blue solid elements are covered, on the top and bottom surfaces, by shell elements, representing the aluminum facesheets.
As the thermal behavior of the PLF is linked to the external airflow, the problems are coupled. The combined solution is obtained through an iterative process (using a loosely coupled two-way approach, described in chapter 3.3.2.3). In it, the thermal FE model, with the solver MSC.NASTRAN, is used to ascertain the unsteady nodal temperatures, which are affected by the radiant, convective and conductive heat fluxes.

3.3 Fluid mechanics models

The Fluid model is needed to determine the aerothermodynamic loads (pressure and heat fluxes distributions) used as inputs for the structural and thermal analyses. To compute the aerothermodynamic loads, two approaches are considered: the first one, referred to as "Semi-empirical", is derived from semi-empirical formulations developed in the '60s. The second approach leverages CFD analyses: computationally, it is significantly more expensive than the first one, but allows to attain a higher level of flexibility and accuracy.
To initialize the Fluid Model, an atmospheric database based on the 1976 U.S. Standard Atmosphere [12] is used.

3.3.1 Semi-empirical

Semi-empirical relations and formulations, expressed for idealized cases, can be extended to the problem at hand. In particular, the formulas are meant to provide a conservative estimate of the aerothermodynamic loads computed for 0° angle of attack.

3.3.1.1 Thermal loads

The thermal loads are computed using the "DKR" (Detra, Kemp, Riddell) formulas [13, 14]. These papers provide generalized formulas to estimate the stagnation heat fluxes q_s for blunt-nosed bodies. Two formulas are defined, respectively valid for the lower part of the atmosphere (where a continuum flow can be assumed) and for the upper part of the atmosphere (where a transitional regime or free molecular flow can be assumed).
For this work, the transition from continuum flow to free molecular flow is assumed to occur at 100 km altitude, at which the Knudsen number Kn is greater than 0.1. In reality, the transition from continuum to free molecular flow is

DOI: 10.13009/EUCASS2022-6129

not abrupt, but actually passes first through the slip flow ($0.01 \leq Kn \leq 0.1$) and then the transitional flow regime ($0.1 \leq Kn \leq 10$). For the Semi-Empirical formulation used for this work, the continuum flow formulation is assumed to hold true for the slip regime as well, while the free molecular flow formulation is used for the transitional flow regime.
It is furthermore important to note that the Semi-Empirical Approach assumes the heat fluxes to be independent of the wall temperatures. In fact, the "DKR" equations are calibrated for a standard launch vehicle and neglect the specific temperature distribution on its surface.
Once the stagnation heat fluxes q_s are known, it is necessary to determine the fluxes distributions over the entire surface of the fairing. To achieve this, the Lees' formulas [15] are used. They permit to estimate the ratio between the local heat flux q and the stagnation heat flux q_s as a function of the hemisphere angle coordinate ϑ, distances along the nosecone (s and s'), freestream heat capacity ratio γ_∞ and freestream Mach number Ma_∞.
After having determined the heat fluxes distributions over the surface of the fairing it is possible to transform them into nodal heat loads, which are then used as inputs for the thermal model described in chapter 3.2.

3.3.1.2 Aerodynamic loads

To obtain the aerodynamic loads distribution, the same approach as for the thermal loads is be used. It is indeed possible to first assess the stagnation pressure loads using the compressible Bernoulli formulations and the work from Cleary [16] is used to estimate the pressure loads distribution over the fairing: starting from the stagnation pressure p_s, the local pressure p decreases linearly over the hemispherical region, reaching the constant value $p / p_s = 0.5$ over the conical skirt (see Figure 10). The resulting impact pressure $p_c = p - p_\infty$ is used as input for the structural analysis.

3.3.2 CFD

The alternative to the Semi-empirical approach is the use of CFD to determine the aerothermodynamic loads (heat fluxes and pressure distributions) over the fairing for a specific set of trajectory-specific freestream conditions and fairing wall temperatures.
For this work, Stanford University Unstructured (SU2) is used as CFD solver [17] to perform steady-state simulations. The use of CFD is based on the continuum flow assumption. For altitudes below 80 km, the flow has been assumed to be fully turbulent, and Reynolds-averaged Navier-Stokes (RANS) equations with Spalart-Allmaras turbulence model have been used. Above 80 km, the flow is assumed to be laminar, due to the very small Reynolds number (Re). Ideal gas model has been assumed for the entire range of altitudes. Regarding the thermal problem boundary conditions, the analyses are run using the isothermal boundary conditions; each analysis assumes that the wall temperature is constant on the entire surface.

3.3.2.1 CFD model limitations

The aforementioned modeling approach contains assumptions leading to approximations of the real flow behavior.
Specifically, the continuum flow model is correct only for the lower regions of the atmosphere: above ~90 km, the Knudsen number can reach values greater than 0.01, generally assumed as the transition between continuum flow regime and slip flow regime. In the slip flow regime, for which $0.01 \leq Kn \leq 0.1$, CFD does not guarantee accurate results; however, for this problem, the approximations introduced by using CFD outside of its validity range do not cause significant discrepancies, as the flow velocities are comparatively low (maximum 3 km/s). These lead to comparatively low stagnation temperatures, and negligible real gas effects in the shock region [18]. Moreover, for similar problems, CFD and Direct Simulation Monte Carlo (DSMC) – state of the art for these conditions – have shown similar results [19, 20].
Similarly, the assumption of fully turbulent flow up to 80 km might yield unrealistic results where the freestream Re is lower than the critical Re (from 50 km upwards). The reason is that the transition from laminar to turbulent might occur not in the immediate proximity of the stagnation point. Considering the flow as fully turbulent in regions where it is still laminar results in an overestimation of the heat fluxes. To provide more reliable results it would be necessary to use a transitional turbulence model for estimating the distance from the stagnation point at which the transition to turbulent flow occurs. Introducing a transitional turbulence model would, however, increase the level of complexity of the problem (due to the unknown surface roughness and freestream turbulence), resulting in a higher time-to-solution. For this work, therefore, transitional turbulence models have been neglected; this choice is backed up by the fact that the heat fluxes predicted by the CFD for this critical altitude region are very close to the heat fluxes predicted by the Semi-empirical approach.
The isothermal boundary condition assumption also introduces some uncertainty, as the temperature of the external wall is practically never uniform. The most accurate way to represent the thermal boundary conditions would be to

DOI: 10.13009/EUCASS2022-6129

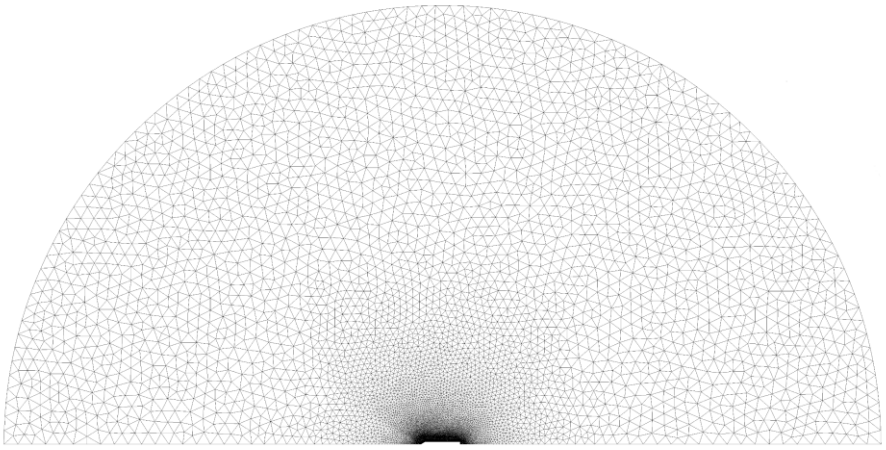

Figure 7: CFD mesh overview

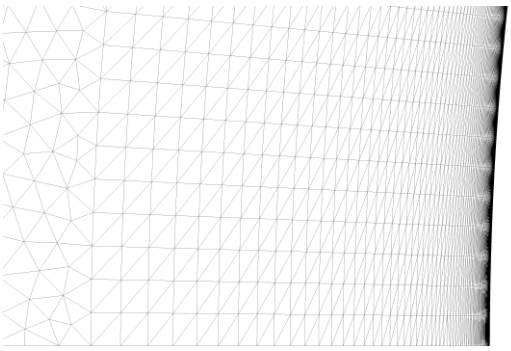

Figure 8: CFD mesh – view of the anisotropic layers

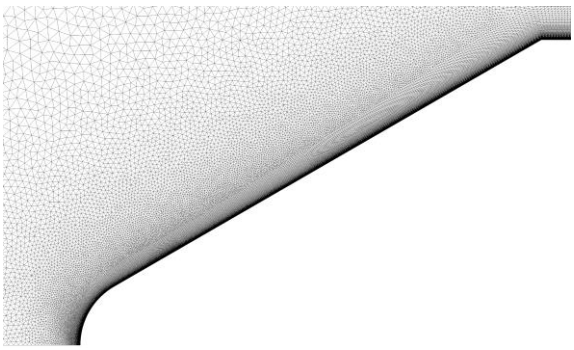

Figure 9: CFD mesh – view of the unstructured domain boundary

define a specific temperature distribution (with a given number of discretizations on the wall surface) for each CFD run. This approach is nonetheless not suited for an optimization as it would require the analysis of thousands of different configurations (a dedicated CFD run would be required for every configuration and for every point along the trajectory) leading to excessive computational costs.

3.3.2.2 CFD Mesh

The mesh used in SU2 is two-dimensional, and is used to run axisymmetric analyses, leveraging the fact that the angle of attack is assumed to be zero throughout the entire trajectory. Although being more time-efficient, using a two-dimensional mesh does not allow to account for three-dimensional phenomena, such as lateral winds or non-zero angles of attack.
The mesh, shown in Figure 7, is hybrid. It consists of layers of anisotropic cells in the near-wall regions (Figure 8), with the rest of the domain meshed in an unstructured manner (Figure 9). The mesh consists of approximately 2 000 000 triangular cells.

3.3.2.3 Aerothermal loads

SU2 directly outputs the pressure distributions and the heat fluxes; these can be directly used as inputs for the thermal and structural analyses. As reference, Figure 10 shows the local pressure ratio p/p_s over the fairing length at 12 km altitude (maximum impact pressures), while in Figure 11 the local heat fluxes ratio q/q_s at an altitude of 45 km is shown.

DOI: 10.13009/EUCASS2022-6129

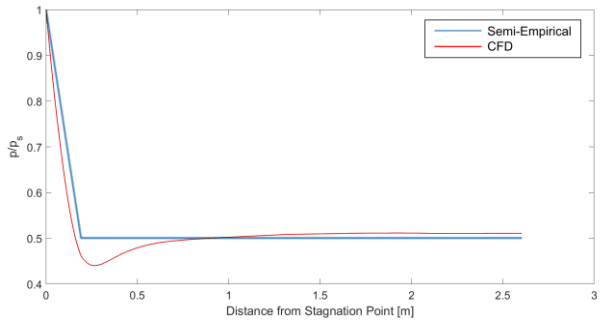

Figure 10: Local pressure ratio over fairing length at 12 km altitude

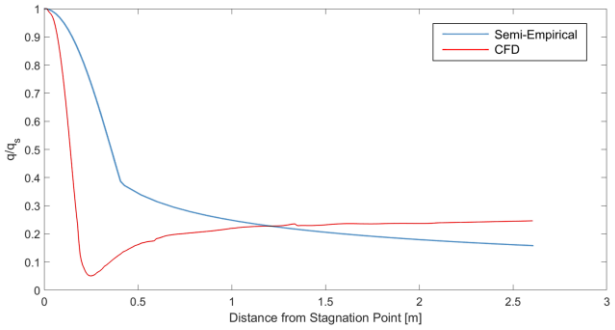

Figure 11: Heat fluxes ratio over fairing length at 45 km altitude

3.4 Costs model

As aforementioned, the cost of both the manufacturing and the refurbishment of the fairing is used as a metric in its optimization. Simplified models have been thus defined to capture the impact of different design parameters on the recurring and refurbishment costs. Specifically, the models include:

- **Raw material costs:** they account for the costs of the aluminum skins, honeycomb core, cork and beams; the specific cost model is based on actual market prices.
- **Processing costs:** they include all the supply-chain and manufacturing costs, hence accounting for the parts procurement or manufacturing, inspection, assembly and integration. The model is based on company data, and accounts for the different logistic costs and assembly complexities associated with manufacturing parts with varying cork, honeycomb core or panels thicknesses.
- **Refurbishment costs:** they model the costs for the refurbishment of the fairing, specifically of the TPS. After each launch, a refurbishment of the TPS must be considered. The extreme cases are with no TPS present (zero costs), and with single-use TPS (high costs, as the entire cork must be replaced and reinstalled). If the TPS can survive multiple flights, the cork can be refurbished with resurfacing. The number of possible reuses for a specific TPS configuration is thus determined by estimating the temperature distribution along its thickness, considering that thermochemical degradation (charring) occurs above 200°C [21]. Each refurbishment cycle removes the charred portion of cork, until the remaining TPS can no longer protect the structure (the elevated temperatures lead to reduced material properties and loss of load-carrying capacity), when it is assumed to be replaced and reinstalled anew. The cost model, considering the associated effort, is based on company data.

3.5 Coupling frameworks

The frameworks couple the different physical domains and models; in the following, three possible workflows are presented.

3.5.1 Iterative framework

The Iterative framework uses CFD to model the aerothermodynamics and Finite Elements Analysis (FEA) to study the structural (mechanical and thermal) behavior, executing one simulation per domain and per timestep.
The aerothermodynamic and the structural thermal domains are two-way weakly coupled. As depicted in Figure 12, a CFD simulation is run (timestep t), yielding the aerothermal loads. These are used as input for the thermal solver. Once the temperature distributions at timestep t are computed, the field is used as input for a new CFD simulation for the next timestep $t + 1$. The outputs are the aerothermodynamic loads at $t + 1$, in turn used as inputs for the thermal model.
The structural model, on the other hand, is one-way weakly coupled with both thermal and fluid domains: the dynamics of the structure are assumed not to affect the aerothermal or structural domain. The structural analysis can be therefore executed after the determination of the pressure and temperature distributions for all timesteps.
The Iterative framework provides a tailored solution for the specific optimization individual which is being studied. In fact, each individual will require CFD to use different boundary condition for the thermal problem (due to a different thermal response of the structure). Whereas this approach would provide the greatest accuracy, it has very high computational costs, making its use impractical in an optimization. For this reason, it was not utilized in the study.

DOI: 10.13009/EUCASS2022-6129

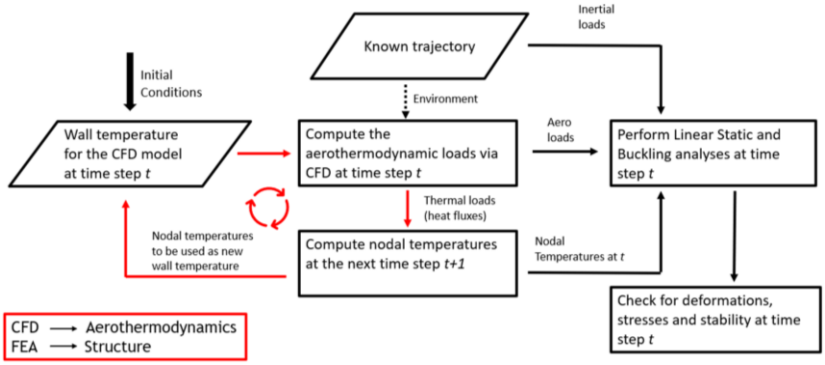

Figure 12: Iterative framework flowchart

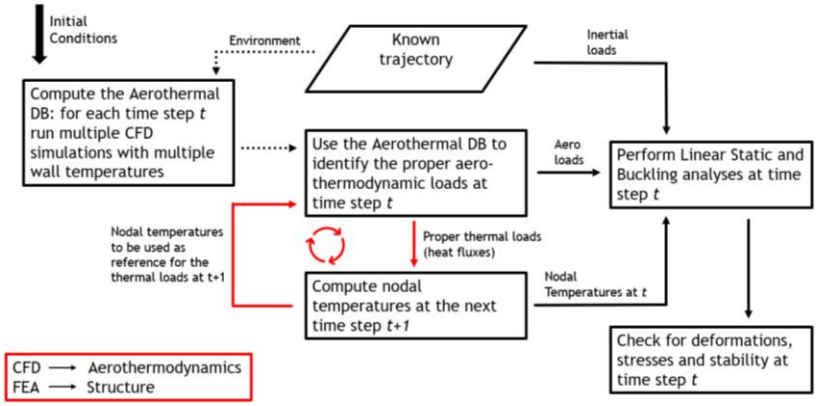

Figure 13: Aerothermal database framework flowchart

3.5.2 Aerothermal database framework

The Aerothermal database framework (Figure 13), like the iterative framework, relies on CFD and FEA models. The difference between the two workflows lies in the CFD analyses, which are only executed for a pre-defined set of uniform wall temperatures[2] and trajectory points. The main assumption is that the aerothermal behavior of the vehicle has low sensitivity with respect to the wall temperature distribution along the fairing.
The thermal solver therefore obtains the thermal flows by polling, for each node, the Aerothermal Database, based on the local wall temperature and position along the trajectory.
Similarly, the pressure distribution is extracted for the structural solver. Although the expected accuracy of this framework is lower than that of the Iterative framework, due to the interpolation process and constant wall temperature assumption, this approach has a significantly lower computational cost, as it requires to perform a limited set of CFD simulations valid for all optimization individuals.

3.5.3 Simplified framework

The Simplified framework (Figure 14) uses the Semi-empirical approach to model the aerothermodynamics and FEA to study the structure. The use of the Semi-Empirical approach reduces the level of complexity of the framework, owing to the absence of bi-directional couplings between any physical domain.
As for the other frameworks, also for this one the structural problem shows no cyclic interface with the fluid model nor with the thermal model. The use of the Semi-Empirical approach, while negatively affecting the overall accuracy (due to the lack of cyclic interaction between the fluid and the thermal models), has a very low computational cost.

[2] specifically, 0°C, 100°C, 200°C, 450°C, 750°C

DOI: 10.13009/EUCASS2022-6129

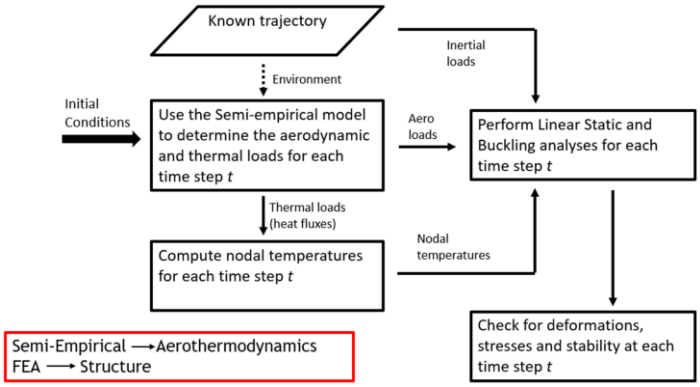

Figure 14: Simplified framework flowchart

3.6 Comparison of models and frameworks

Considering the coupling between the fluid domain and the other domains, it is necessary to evaluate how the presented coupling frameworks compare. This is performed by comparing the predicted pressure and heat fluxes distributions, and the consequent temperature distributions on the structure.

Figure 15 compares the stagnation point impact pressures computed through the Semi-empirical and CFD approaches, showing excellent coherence between the two models, not only in terms of relative errors, but also with respect to the prediction of the maximum impact pressure flight altitude (estimated at 12 km).

With respect to the pressure distributions over the fairing's height, it is possible to compare the curves in Figure 10. The simple modelling provides a conservative pressure distribution, since it does not consider the pressure drop caused by the transition from the hemispherical part of the nose cap region to the conical section (due to impact of pressure gradients on the boundary layer), not constant and function of the flight condition.

Figure 16 compares the stagnation point heat fluxes. It is important to note that the heat fluxes computed using the Semi-empirical model are independent of the wall temperatures. Consequently, they are identical for every

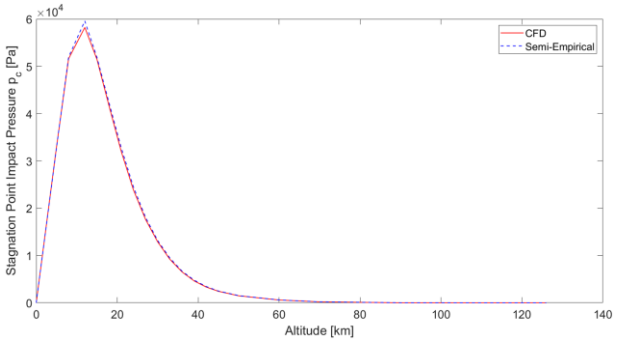

Figure 15: Comparison between the stagnation point impact pressures predicted by the Semi-empirical and CFD models

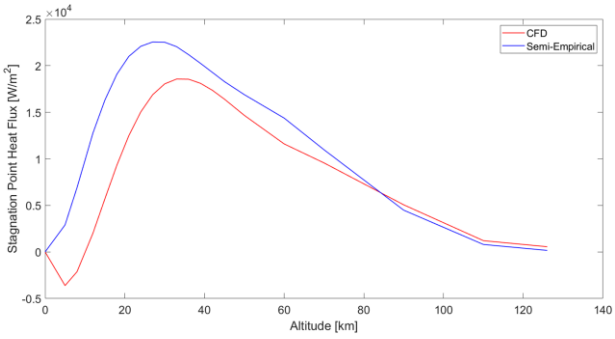

Figure 16: Comparison between the stagnation point Heat Fluxes predicted by the Semi-empirical and CFD models

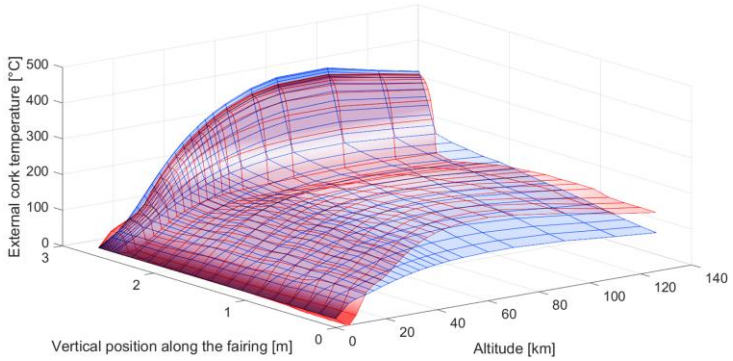

Figure 17: TPS temperatures as a function of altitude and vertical position along the fairing, calculated using the simplified (blue) and aerothermal database (red) frameworks

DOI: 10.13009/EUCASS2022-6129

optimization individual. This is not the case for the heat fluxes computed using CFD, which depend upon the wall temperature, function of thermal properties of the fairing structure.
Despite these limitations, the plot shows similar trends for altitudes above approximately 30 km. The Semi-empirical approach is indeed tailored to study supersonic and hypersonic flight conditions and serves as a conservative reference until 90 km altitude, where the CFD Approach predicts higher heat fluxes. At high altitudes, however, the CFD results have higher uncertainty, owing to the high *Kn* number of the flows and to the ideal gas assumption.
With respect to the heat fluxes distributions over the fairing's height, the Semi-empirical method predicts a cosinusoidal distribution over the nose cap [15], which is also shown by the CFD results (Figure 11). As already observed for the pressure distributions, the Semi-empirical method does not account for the heat fluxes drop caused by the transition from the hemispherical region of the nose cap to the conical skirt section.
To evaluate the impact of using different methods and different coupling frameworks, it is possible to compare the resulting temperature distribution of the fairing, of primary interest in the study. Figure 17 compares the external cork temperature distributions for the entire fairing surface and for the entire trajectory, computed with the Aerothermal database and the Simplified frameworks, for a standard fairing configuration.
The predicted temperatures in the nose cap region are very similar, not only in terms of peak values (slightly higher for the simplified framework), but also in terms of the trend, with the maximum located at the same altitude. It is furthermore interesting to notice that, for both frameworks, the altitudes at which the skirt and the nose cap experience peak temperature are different. With respect to the conical skirt region, on the other hand, the frameworks predict a different behavior, owing to the differences in the predicted heat flux distributions. Whereas the Simplified framework shows monotonically decreasing temperatures moving away from the stagnation point, the Aerothermal database shows a temperature drop in the initial part of the conical skirt followed by a moderate increase along its length.

4. Multi-disciplinary optimization

The Multi-Disciplinary Optimization (MDO) environment for this work is schematically depicted in Figure 18. It links three blocks: the optimizer, the Multi-disciplinary Design Analysis (MDA) block and the objective function block. Given the design variables, the performance metrics of the individual, directly related to the results of the analyses in the various disciplines, are computed by the MDA block. They are used, together with the constraints, to determine the objective functions.
The Multi-disciplinary Design Analysis block represents the interaction between disciplines, and consists of the Aerothermal database framework and the Simplified framework, described in chapters 3.5.2 and 3.5.3. In addition to evaluating the maximum temperature, strength and stability of the structure, according to the requirements defined in Table 1, they evaluate the mass and lifecycle cost of the individual.
The optimization algorithms used in this study are CMA-ES [22] for single-objective optimizations and MO-CMA-ES [23] for multi-objective studies. They belong to the class of evolutionary algorithms, and are well suited for non-linear, non-convex problems in continuous domains. They define each candidate individual through a set of design variables (described in chapter 2.3), and they evaluate the resulting fitness using the results of the multi-disciplinary analysis. The fulfilment of the constraints is enforced by penalizing, in case of non-compliances, the objective function(s).
The objective functions, in turn, differ according to the type of optimization, namely whether it is single- or multi-objective. In the first case, a linear scalarization [24] is used, weighting and adding the individual contributors (specifically, mass and total lifecycle cost) to determine the objective function; the optimal individual will therefore depend upon the choice of weights. Given the specific objective functions, this equates to assigning a monetary cost to the PLF mass. In the second case, the fitness functions are directly the physical quantities mass and total lifecycle cost, and the result of the optimization will be a set of Pareto-optimal individuals.

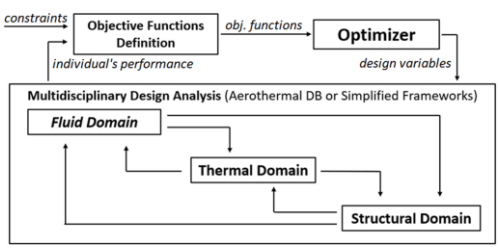

Figure 18: MDO flowchart

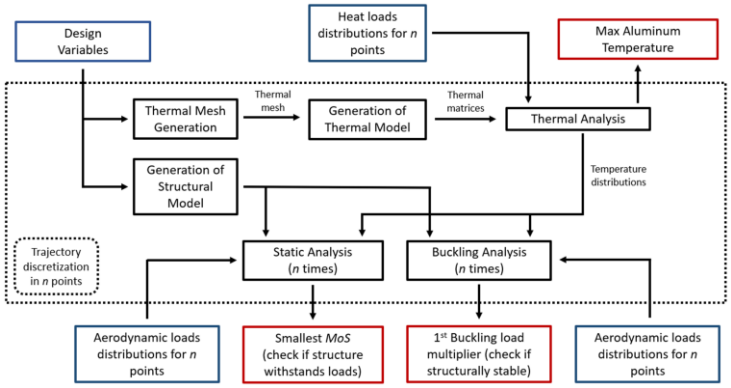

Figure 19: Multi-disciplinary Design Analysis flowchart

DOI: 10.13009/EUCASS2022-6129

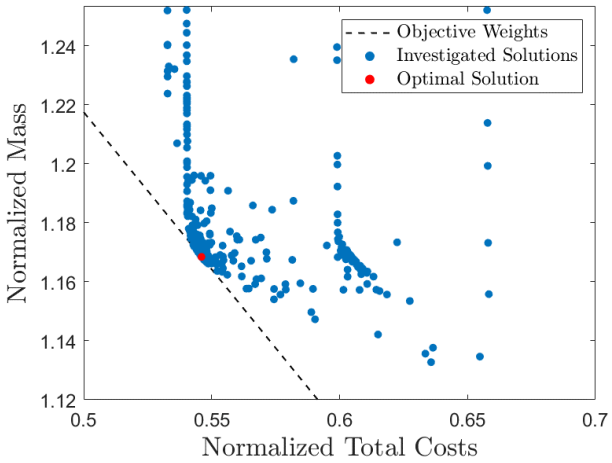

Figure 20: TPS sizing optimization results

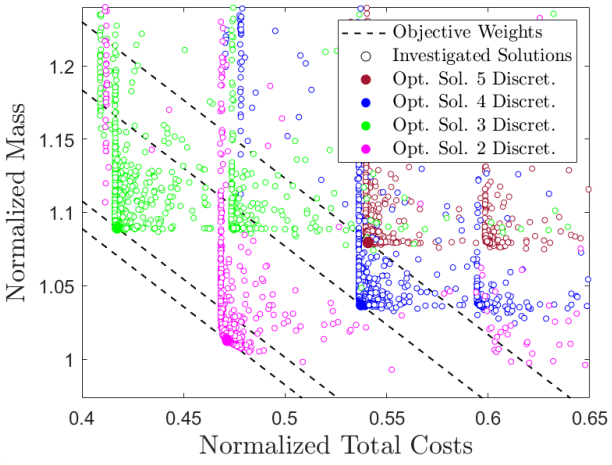

Figure 21: Thickness discretization optimization results

For this study, the design parameters are related to the structure (listed in chapter 2.3.1) and to the TPS (listed in chapter 2.3.2). The constraints (listed in Table 1) express the necessity, from a structural perspective, to have sufficient margin of safety for the static strength, and sufficiently high buckling factor to ensure stability. From a thermal perspective, they ensure that both maximum structural temperature and maximum irradiation are below a threshold.
The objective functions, as aforementioned, are the mass of the fairing and the total lifecycle cost. Specifically, all studies assume the need for 10 re-uses of the structure, hence resulting in a total of 10 refurbishments (or replacements) and 11 flights.
In the following paragraphs, in addition to a global optimization (chapter 4.3), the impact of specific design parameters (e.g. cork thickness) on the performance are presented. By restricting the search space of the optimizer (for example, limiting it only to TPS-related parameters), it is possible to identify design guidelines for a specific aspect (for example, how the TPS sizing impacts the reusability).

4.1 TPS sizing

The optimization can be used to assess the ideal sizing for the TPS (results shown in Figure 20), given a specific structural configuration. The design variables are related to the cork thicknesses variation along the fairing's height.
The optimal solution, identified using the aerothermal database, has a total mass 1.17× greater than that of the non-reusable, reference configuration and total lifecycle costs, equal to 55% of those of the reference configuration. The optimal configuration achieves six flights (hence five refurbishments) without replacement of the skirt TPS, where the outer temperature reaches a maximum of 205°C, resulting in a structural temperature of approximately 100°C. On the other hand, the nose-cap cork section reaches 393°C, must be replaced after each flight, and its sizing is defined by the maximum allowable temperature of the structure. The refurbishment costs associated with the nose cap section are indeed rather small, therefore the optimizer outputs solutions with non-reusable nose cap cork panels.
Figure 20 shows additionally the presence of a local minimum, caused by the definition of the refurbishment costs: these are based on the finite number of times that a specific TPS configuration is reusable without replacement (chapter 3.4); the local minimum has a different number of maximum reuses, leading to a worse overall performance.

4.2 Thickness discretizations

As described in chapters 2.3.1 and 2.3.2, the thickness of the structural and TPS components is assumed to be variable in steps, along the height of the PLF. A finer discretization, hence with constant-thickness areas of smaller dimensions, permits in principle to attain lower mass; however, owing to the greater logistic efforts associated with procuring, finishing and installing panels of different thicknesses, the costs would also be higher (see chapter 3.4). Four separate single-objective optimizations have been executed, using the aerothermal database, to assess the impact of this parameter on the mass and cost.
Figure 21 shows widely varying normalized masses and costs for the four optimal solutions; this is due to the use of single-objective optimizations to perform this study, which identifies an optimal solution according to the specific choice of weights. Nonetheless, the comparison of single-objective analyses still allows to draw conclusions for this weighting scenario: the best configurations are the ones with 2 and 3 thickness discretizations. In fact, although the two configurations have a completely different approach to reusability (the design with 2 discretizations has a skirt that lasts two reuses, whereas that of the design with 3 discretizations lasts six flights, leading to a high mass for the TPS),

DOI: 10.13009/EUCASS2022-6129

they possess the smallest costs. The specific objective weighting, favoring low overall costs, are unfavorable for configurations with high number of discretizations, characterized by high manufacturing and refurbishment costs.

4.3 Multi-objective optimization

Allowing the optimizer to vary all design parameters, hence maximizing the search space, permits in principle to identify the optimal solution. By performing multi-objective optimizations, no arbitrary weighting between objectives is prescribed; the solution therefore consists of a set of designs, Pareto-optimal in terms of mass and total cost.
This study considers five discretizations for the thickness (therefore giving the greatest design freedom to the optimizer). The analysis is performed with both Simplified and Aerothermal database frameworks, permitting to compare the impact of the approximations of the former framework on the final design. The optimization results are shown in Figure 22; for completeness, the results of a single-objective optimization (marked S-O) using the Aerothermal Database framework are included. The Pareto fronts obtained by both models are very similar, and both frameworks show a non-convex front with a stepped shape. As mentioned in chapter 4.1, the reason for this trend lies in the definition of the total costs, linked to the discrete nature of the maximum refurbishments the fairing cork panels can withstand.
For comparison purposes, seven individuals on the Pareto front of the Aerothermal Database optimization are evaluated, and selected design parameters and reusability characteristics are summarized in Table 2.
On the left side of the front, where individual 1 lies, the optimal solution has the highest degree of reusability, employing a layer of cork so thick that it can withstand repeated charring and resurfacing (hence characterized by higher mass). Moving downwards along the Pareto front, the degree of reusability decreases, and so does the maximum cork thicknesses. The configuration on the right side of the Pareto front has limited reusability, but lowest mass.
The configurations in the middle of the Pareto front show a tradeoff between mass and costs, possessing a certain level of reusability. In particular, with a 72% skirt cork thickness increase with respect to the reference non-reusable configuration, it is possible to use the skirt TPS for six flights (individual 5). To achieve full reusability for the skirt section, a cork panel at least 3.60 times thicker than the reference must be employed.
The optimization results obtained using the two different frameworks shows similar trends, although the simplified framework identifies lighter solutions. This is a consequence of the different fluid-dynamic modelling which, as discussed in chapter 3.6, predicts lower heat fluxes on the skirt section (thus requiring lower TPS thicknesses).
In comparison to the single-objective solution (obtained using the Aerothermal Database framework), the multi-objective Pareto-optimal individuals show slightly worse performance. The rationale is the slower convergence characteristics of the multi-objective optimization with respect to the single-objective one: with more iterations, the multi-objective optimization is expected to identify the same optimum.

Table 2: characteristics of selected Pareto-optimal individuals

Indiv.	Nose cap TPS: max. flights count	Skirt TPS: max. flights count	Min. cork thickness (normalized)	Max. skirt cork thickness (normalized)	Max. nose cap cork thickness (normalized)
1	6	11	0.94	4.73	5.67
2	4	11	0.94	3.60	4.27
3	3	8	0.96	2.87	3.32
4	2	7	0.99	2.08	2.34
5	1	6	1.01	1.72	1.89
6	1	4	1.04	1.38	1.47
7	1	3	1.07	1.32	1.39

DOI: 10.13009/EUCASS2022-6129

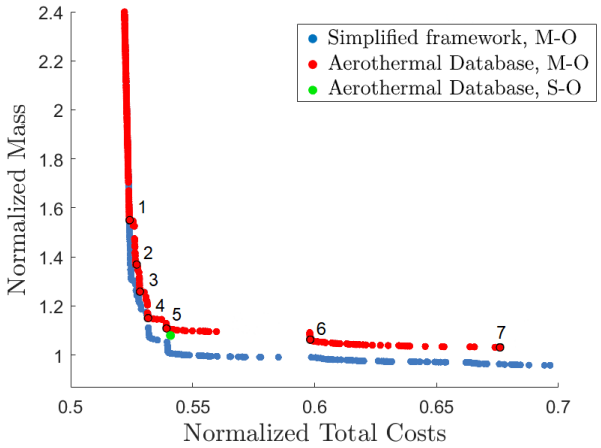

Figure 22: Single- and multi-objective optimization results, using different frameworks

5.Conclusions and outlook

A multi-disciplinary optimization environment has been developed aiming at investigating the complex and multi-faceted nature of the conceptual design phase of a payload fairing, where multiple physical domains couple with each other. To provide a comprehensive view on the problem, two separate frameworks, based on different fluid-structure interaction philosophies, have been used to run the optimization analyses: the first one being less computationally demanding, based on the use of semi-empirical formulations to describe the fluid domain; the second one, more computationally expensive, studying the aerothermodynamics using CFD.

The optimization results obtained with the two methods show good consistency, proving the possibility of using low-fidelity models to correctly interpret the physics involved in the conceptual design phase of such complex systems.

This work also showcases the potential of using MDO at the initial phases of the project development: considering the level of uncertainty associated to the initial stages of any new project, and therefore the chances of making incorrect initial decisions or assumptions, a multi-disciplinary optimization environment allows to flexibly re-adapt the analysis to new requirements, allowing in such a way to quickly iterate and converge towards an optimal solution. The possibility of extracting design guidelines, even for unconventional concepts and considering the interplays between disciplines, enables to establish the ideal design space at an early phase. Furthermore, owing to the increased accuracy of modelling tools and guidelines derived from them with respect to conventional design criteria, uncertainties are reduced, decreasing the risk of deviations (and thus time and cost overruns) in subsequent project phases.

This is especially important when considering components reusability and the trend towards cost effectiveness: heritage design approaches and structural concepts might not provide the best solution, whereas an unbiased optimization can return a set of optimal (albeit possibly unconventional) results.

As a response to the market evolution, it would be valuable to analyze the sensitivity of the analyses performed in this work (for example using Monte Carlo methods or Polynomial Chaos-based approaches) with respect to the multiple parameters and assumptions, with major focus on the costs definition and their impact on the final design. With the ever-changing market situation, it would indeed be relevant to understand how cost uncertainties (e.g. costs of materials) might propagate and ultimately influence the optimal solution.

Moreover, as already stated, this work aims at providing a systematic approach to examine the design phase of a fairing on a conceptual/preliminary level. Nonetheless, the same philosophy could be embraced to adapt the optimization environment to a detailed level analysis. This could be achieved for example by including a family of trajectories in the optimization environment, by analyzing and optimizing different fairing geometries, by assessing different materials and construction techniques, by devising more realistic structural concepts with corresponding design parameters, by refining the fluid dynamic models or by even considering other modeling approaches, such as the use of Direct Simulation Monte Carlo to study the aerothermodynamics.

References

[1] J. Blair, R. Ryan, L. Schutzenhofer and W. Humphries, "Launch Vehicle Design Process: Characterization, Technical Integration, and Lessons Learned," NASA / TP-2001-210992, 2001.

[2] Federal Aviation Administration, "The Annual Compendium of Commercial Space Transportation: 2018," FAA AST, 2018.

DOI: 10.13009/EUCASS2022-6129

[3] Hexcel, "HexWeb® CR III Product Data Sheet," Hexcel Corporation, 2017.

[4] J. K. Paik, A. K.Thayamballi and G. S. Kim, "The strength characteristics of aluminum honeycomb sandwich panels," *Thin-Walled Structures,* vol. 35, no. 3, pp. 205-231, 1999.

[5] J. Smith, "Evolved Composite Structures for Atlas V," in *38th AIAA/ASME/SAE/ASEE Joint Propulsion Conference & Exhibit*, Indianapolis, Indiana, 2002.

[6] F. Shen and D. Pope, "Design and Development of Composite Fairing Structures for Space Launch Vehicles," in *Aerospace Technology Conference and Exposition*, Long Beach, CA, 1990.

[7] R. N. Shama, T. G. A. Simha, K. P. Rao and G. V. V. Ravi Kumar, "Carbon composites are becoming competitive and cost effective," Infosys, 2018.

[8] I. Sakraker, O. Chazot and J. P. Carvalho, "Performance of cork-based thermal protection material P50 exposed to air plasma," *CEAS Space Journal,* vol. 14, p. 377–393, 2022.

[9] J. Randolph A. Graves and J. Thomas E. Walton, "Free-flight test results on the performance of cork as a thermal protection material," NASA, Washington, DC, 1964.

[10] R. Beck and D. Davis, "Fundamentals of Ablative Thermal Protection Materials," in *Thermal and Fluid Analysis Workshop (TFAWS)*, Huntsville, AL, 2017.

[11] W. Ley, K. Wittmann and W. Hallmann, Handbook of Space Technology, John Wiley & Sons, Ltd, 2011.

[12] NOAA; NASA; USAF, "U.S. Standard Atmosphere," U.S. Government Printing Office, Washington, D.C., 1976.

[13] R. Detra and H. Hidalgo., "Generalized heat transfer formulas and graphs for nose cone re-entry," *ARS Journal,* vol. 31, no. 3, pp. 318-321, 1961.

[14] N. H. Kemp and F. R. Riddell, "Heat transfer to satellite vehicles re-entering the atmosphere," *Journal of Jet Propulsion,* vol. 27, no. 2, pp. 132-137, 1957.

[15] L. Lees, "Laminar Heat Transfer Over Blunt-Nosed Bodies at Hypersonic Flight Speeds," *Jet Propulsion Archive,* vol. 26, no. 4, pp. 259-269, 1956.

[16] J. W. Cleary, "An Experimental and Theoretical Investigation of the Pressure Distribution and Flow," NASA, Washington, DC, 1965.

[17] F. Palacios, J. Alonso, K. Duraisamy, M. Colonno, J. Hicken, A. Aranake, A. Campos, S. Copeland, T. Economon, A. Lonkar, T. Lukaczyk and T. Taylor, "Stanford University Unstructured (SU²): An open-source integrated computational environment for multi-physics simulation and design," in *51st AIAA Aerospace Sciences Meeting*, Grapevine, TX, 2013.

[18] M. S. Ivanov and S. F. Gimelshein, "Computational hypersonic rarefied flows," *Annual Review of Fluid Mechanics,* vol. 30, no. 1, pp. 469-505, 1998.

[19] V. K. Dogra, J. N. Moss, R. G. Wilmoth, J. C. Taylor and H. A. Hassan, "Effects of chemistry on blunt-body wake structure," *AIAA Journal,* vol. 33, no. 3, pp. 463-469, 1995.

[20] J. N. Moss, J. M. Price and V. K. Dogra, "DSMC Calculations for a 70° Blunted Cone at 3.2 km/s in Nitrogen," NASA, Hampton, VA, 1995.

[21] H. Pereira, "The thermochemical degradation of cork," *Wood Science and Technology,* vol. 26, pp. 259-269, 1992.

[22] N. Hansen and A. Ostermeier, "Adapting arbitrary normal mutation distributions in evolution strategies: The covariance matrix adaptation.," in *IEEE International Conference on Evolutionary Computation*, Nayoya University, Japan, 1996.

[23] C. Igel, N. Hansen and S. Roth, "Covariance Matrix Adaptation for Multi-objective Optimization," *Evolutionary Computation,* vol. 15, no. 1, pp. 1-28, 2007.

[24] C.-L. Hwang and A. S. M. Masud, Multiple Objective Decision Making — Methods and Applications, Berlin: Springer Berlin, Heidelberg, 1979.

[25] ArianeGroup, "VEGA C user's manual," 2018.

[26] G. A. Bird, Molecular Gas Dynamics and the Direct Simulation of Gas Flows, Clarendon Press, 1994.